



Conductive, Anti-Corrosion, Self-Healing Smart Coating Technology Incorporating Graphene-Based Nanocomposite Matrix

Jaime Benavides-Guerrero, Debika Banerjee, Dawit Gedamu, Luis Felipe Gerlein and Sylvain G. Cloutier*

Department of Electrical Engineering, École de technologie supérieure, Montreal, QC, Canada

OPEN ACCESS

Edited by:

Zhihui Xie,
China West Normal University, China

Reviewed by:

Yunze Xu,
Dalian University of Technology, China
Jihu Wang,
Shanghai University of Engineering
Sciences, China

*Correspondence:

Sylvain G. Cloutier
sylvain.g.cloutier@etsmtl.ca

Specialty section:

This article was submitted to
Smart Materials,
a section of the journal
Frontiers in Materials

Received: 15 December 2021

Accepted: 16 March 2022

Published: 31 March 2022

Citation:

Benavides-Guerrero J, Banerjee D,
Gedamu D, Gerlein LF and Cloutier SG
(2022) Conductive, Anti-Corrosion,
Self-Healing Smart Coating
Technology Incorporating Graphene-
Based Nanocomposite Matrix.
Front. Mater. 9:835855.
doi: 10.3389/fmats.2022.835855

Chromate conversion coatings have been in service for decades providing robust corrosion protection to a wide variety of aluminum alloys. However, it is also known that anti-corrosive coatings containing Cr^{6+} contributes to DNA damage, cause cancer and are not environmentally friendly. Consequently, regulatory restrictions over the use Cr^{6+} were established to mitigate the environmental damage and health problems. To answer to this hurdle and to meet the emergent need for environmentally friendly anti-corrosive coatings, we have successfully developed an innovative coating that combines anti-corrosive, low electrical resistance, and self-healing properties. First, we present two different coatings, that aim to display low electrical resistance properties: one containing only graphene and the other containing Zn nanoparticles and graphene. Confocal laser imaging and SEM microscopy was used to observe the morphology of the coatings. The electrical resistance was measured using the 4-wire connection Kelvin method. We compare the anticorrosive response for both coatings under neutral salt spray test (NSSt). Raman spectroscopy was performed before and after to understand the effect of NSSt corrosive species on the coatings. Then, we select the coating with lower electrical resistance, and we program on it a self-healing mechanism to boost its life service. Finally cyclic voltammetry is performed to confirm the excellent blocking properties of the tested coatings. All the coatings presented in this work are applied on aluminum AA 2024T351 and the optimal spray parameters for nanofillers dispersion are obtained. Our findings show great potential for preventing corrosion and compatibility with fully automated large-scale applications in different fields such as aerospace, automotive, construction, submarines and many more.

Keywords: anti corrosion coatings, UV curable, graphene, self-healing, chromium (VI), aerospace, conductivity

1 INTRODUCTION

All metals are susceptible to corrosion and like other natural hazard, corrosion causes severe and expensive damage (Hamdy Makhoulf, 2014; Hou et al., 2017). Corrosion varies according to several factors. Among the most relevant are the corrodent's nature which can be wet or dry (Hamdy Makhoulf, 2014), the corrosion mechanism that may occur as a direct chemical or electrochemical reaction (Hamdy Makhoulf, 2014) and finally, the appearance of the corroded metal (Heusler et al., 1989; Hamdy Makhoulf, 2014). Strategies to prevent corrosion are essentially based on the understanding of these factors and the synergy between them (Hamdy Makhoulf, 2014).

One of the most popular strategies to protect aluminum and other metals from corrosion is the use of coatings. Anti-corrosive coatings can be organic, non-metallic inorganic, and metallic (Hamdy Makhoulf, 2014). There are three mechanisms that provide anti-corrosive properties in coatings: acting as a blocking layer, acting as an inhibition layer and acting as a sacrificial layer (Hamdy Makhoulf, 2014). In this work we use an equilibrated combination of these three mechanisms.

Aluminum alloys are widely used for aerospace applications due to its advantageous weight-to-strength ratio (Mondolfo, 2013). Generally, these aluminum alloys are protected against corrosion with metallic coatings such as hexavalent chromium (Cr^{6+}) conversion coatings. The use of coatings based on Cr^{6+} is common in the aerospace industry since it is extremely thin, usually in the range of nanometers (Katzman et al., 1979), a desirable feature that adds minimal weight to the structure while providing a robust corrosion protection (Kendig and Buchheit, 2003). Moreover, chromate conversion coatings have been in service for decades protecting different metals from corrosive environments (Davis, 1999; Chou et al., 2003; Hamdy Makhoulf, 2014). Nevertheless, it is been proved that coatings containing Cr^{3+} and Cr^{6+} contributes to DNA damage, cause cancer and are environmentally unfriendly (O'Brien and Kortenkamp, 1995). In consequence, restrictions and regulatory policies are in place to replace Cr^{6+} conversion coatings.

In response, different less toxic alternatives to Cr^{6+} have been investigated, for instance, salts (Nazeer and Madkour, 2018) such as silicate, molybdate, vanadate, permanganates, zirconates, and ceria (Hamdy and Beccaria, 2005; Hamdy, 2006; Hamdy et al., 2011, 2012; Makhoulf and Tiginyanu, 2011) were found to be inexpensive, environmentally safe and provide self-healing properties. These salts are usually applied directly to create a protective oxide layer that passivates the aluminum (Hamdy, 2007, 2008; Hamdy and Farahat, 2010). Once the passivation is done, the anticorrosive organic/inorganic coating is applied on top (Nazeer and Madkour, 2018). Another interesting approach is the use of self-assembled coatings based on the chemisorption of sodium monododecyl phosphate from aqueous solution. This approach showed improvement in the corrosion resistance of treated aluminum alloys exposed to corrosive Cl^- atmospheres (Pan et al., 2020; Xia et al., 2020)

In the same way, several materials have been used as matrices for anticorrosion coatings (Metroke et al., 2002; Jang, 2006; Sørensen et al., 2009; Zang et al., 2014). Among those

materials, sol-gel organic modified silica (ormosil) coatings present themselves as a good candidate to develop anticorrosive coatings capable to replace Cr^{6+} coating technology (Metroke et al., 2002; Pagliaro et al., 2009; Smitha et al., 2018). They are interesting not only for its rapid and relatively easy synthesis (Mackenzie and Bescher, 1998; Han et al., 2007) but also because its chemistry allows for UV-polymerization (Han et al., 2007; Gvishi et al., 2012). Indeed, UV-curing anticorrosive coatings are desirable to protect aerospace aluminum parts that cannot be expose to high temperatures to avoid deformation. The downside is that sol-gel coatings are well hydrated at the beginning of its service-life, but their coating properties change drastically as they are exposed to the elements. In consequence there is a loss on its corrosion resistance and adhesion properties (Kendig and Buchheit, 2003).

Moreover, the need for multifunctional coatings capable to display both, corrosion protection and low electrical resistance is relevant for aircraft and spacecraft industries (Larsson, 2002). Indeed coatings with these properties are well suited for electrostatic dissipation (Yadav et al., 2020), electromagnetic shielding (Aal et al., 2008) and lightning strike protection (Kim et al., 2019). To serve as intended, the thickness coatings should be tailored precisely. I.e., thick enough to provide excellent barrier properties and thus excellent anticorrosive response, but not too thick that it will disrupt the conductive path. In other words, having anti-corrosion and low electrical resistance in the same coating is useful and desirable but is a challenging task since several parameters need to be orchestrated and most importantly, these two properties are antagonistic in nature (Shi et al., 2009).

Bringing conductive or low electrical resistance properties to sol-gel anticorrosive and UV-curable coatings has been attempted by dispersing conductive nanofillers within the sol-gel matrices. Unfortunately, it was shown that this incorporation cause a negative effect on the achieved anticorrosive properties since the fillers compromise the mechanical and barrier properties of the coatings creating local defects and provide an electrical path for corrosion to take place (Zhang Q. et al., 2018; Agustín-Sáenz et al., 2020; Tian et al., 2021).

On the other hand, polymer matrices are well known for their stability and anti-corrosive properties (Barsoum and Barsoum, 2002; Kim et al., 2019). Contrary to sol-gel, the addition of different kinds of nanoparticles to polymeric coatings improve the coating's anti-corrosive response (Shi et al., 2009) and enables new features such as low electric resistance or self-healing properties (Tiwari et al., 2014). These new features expand the range of applications, service-life and brings innovative solutions to this well-developed market.

In this work we use a UV-curable polymeric resin NOA73 from Norland Optics as an anti-corrosive matrix where we disperse graphene as a conductive filler. In fact, UV-curable resins such as thiol-ene based polymers are attractive to replace chromate conversion coatings (Park and Braun, 2010; Wang et al., 2018, 2019) since they offer insulative properties, long term stability, easy implementation and low curing temperatures (Park and Braun, 2010).

The information presented in this manuscript is the result of a joint venture between ÉTS and Arianegroup. As such, there were

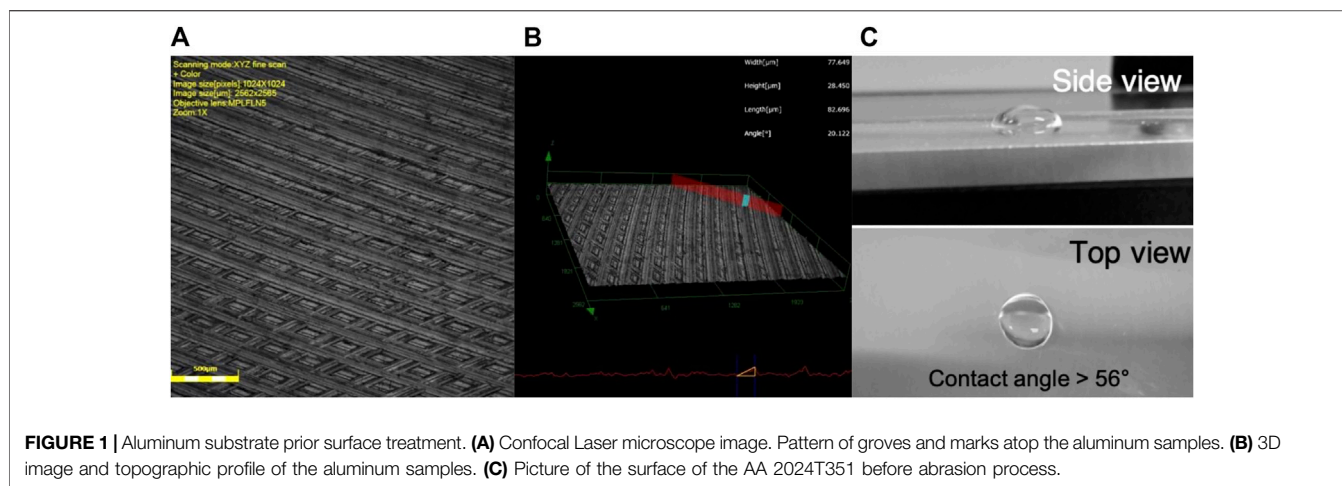


FIGURE 1 | Aluminum substrate prior surface treatment. **(A)** Confocal Laser microscope image. Pattern of grooves and marks atop the aluminum samples. **(B)** 3D image and topographic profile of the aluminum samples. **(C)** Picture of the surface of the AA 2024T351 before abrasion process.

specific requirements on the thickness, anti-corrosive and electrical properties that directed the development and research approach. In this paper, we present the electrical, anti-corrosive and self-healing response of a maximum 10 μm thick NOA73 coating doped with graphene flakes and zinc (Zn) nanoparticles and 8-hydroxyquinoline (8HQ) as self-healing agent. The goal of this work is to develop a sophisticated low-temperature or UV-curable coating technology as an option to the actual anticorrosive coatings used in the aerospace industry, all this in compliance with the international environmental regulations.

2 MATERIALS AND METHODS

2.1 Aluminum AA 2024T351 Surface Preparation and Characterization

Aluminum samples AA 2024T351 were purchased from HRT Industries Inc. Using a 3D confocal laser microscope, we perform a surface analysis of the samples before and after the mechanical abrasion and 3D reconstruction.

2.1.1 Original Aluminum Samples

The surface of the aluminum AA2024 samples as received presents grooves and imperfections left by the machining procedure (Figure 1).

These grooves generate imperfections all over the aluminum surface. The highest defects can be found in the intersections of the machining marks. These can be as high as 28 μm . The surface roughness parameter R_a for the as received aluminum samples is 0.998 μm . Moreover, the surface of the as received AA 2024T351 shows a contact angle with water $>56^\circ$.

2.1.2 Abraded Samples

To obtain a uniform surface, mechanical abrasion was carried out. First the samples are cleaned with ethanol to remove grease and dust. Then, they are abraded using deionized water and alternating in X and Y direction using a 3M7447 general purpose hand pad. Finally, the abraded aluminum samples are rinsed with deionized water and cleaned with a piece of cloth.

A closer inspection of the abraded aluminum sample reveals a reduction in the height of the defects. In fact, after the mechanical abrasion, the height of the defects was reduced from 28 to 4.47 μm and the contact angle was reduced to $<28^\circ$ (Figure 2). The surface roughness parameter R_a for the abraded aluminum samples is 1.058 μm . The elemental composition of the cleaned AA 2024T351 samples was obtained by energy dispersive x-ray analysis (EDAX) and is shown in Table 1.

2.2 NOA73 Matrix Characterization

In this work we use NOA73 resin as the host matrix for the coating. NOA73 is a commercial thiol-ene based resin. We choose it mainly for its anticorrosive properties and for its compatibility with the current aircraft and spacecraft industrial requirements such as spray gun deposition, low curing temperature or UV-curing, strong adhesion to metals, low shrinkage and gap filling properties (Park and Braun, 2010). We performed Raman spectroscopy and FTIR analysis of NOA73 to obtain information and identify its composition and curing mechanism (Figure 3).

As such, we observe that the decrease in intensity of the FTIR band at 2,572 cm^{-1} (Figure 3A) after UV-curing shows characteristic bond between thioleues and allyl ethers (Nagarjuna et al., 2018). Based on the obtained Raman spectra of cured NOA73 (Figure 3B) and taking into account the findings reported in the literature (Mongkhontreerat et al., 2013), we can conclude that the main components in NOA73 are triallyltriazinetrione and tris [2-(3-mercaptopropionyloxy)ethyl]isocyanurate in a molar proportion of at least 1:5, using 2,2-dimethoxy-2-phenyl- acetophenone as photoinitiator and triallyl isocyanurate as crosslinking catalyst (Sanoria et al., 2015).

Based on this information, the anticorrosion (Park and Braun, 2010) properties of NOA73 are expected since it is known that sulfur-rich hyperbranched polyols as the tris [2-(3-mercaptopropionyloxy)ethyl]isocyanurate combined with thiol-ene polymers such as triallyltriazinetrione exhibit high transparency, high refraction index and most importantly, high corrosion resistance (Ireni et al., 2016; Resetco et al., 2017).

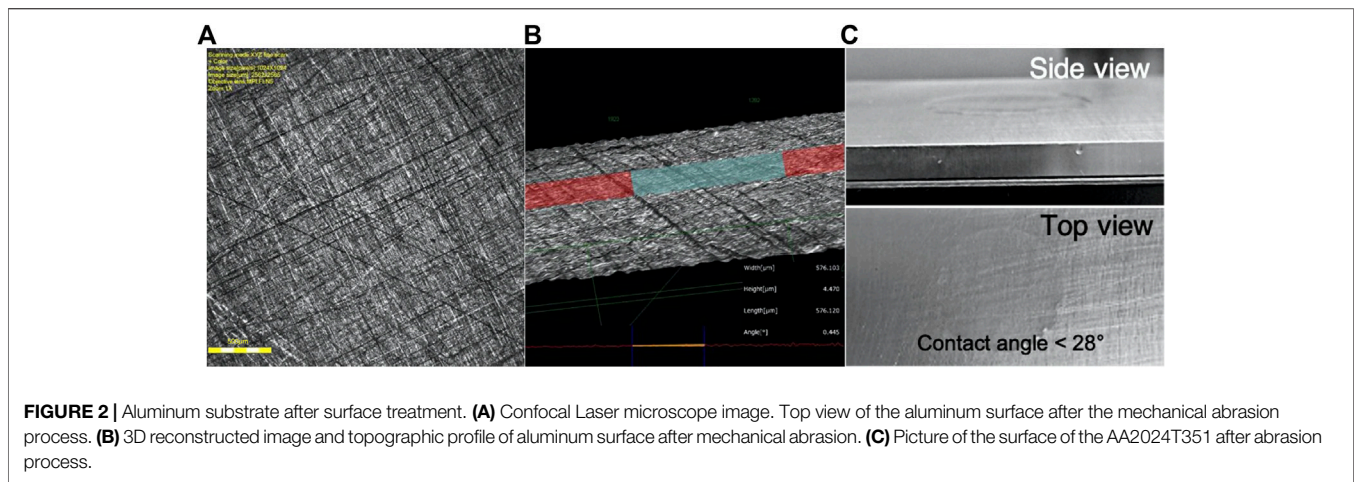


FIGURE 2 | Aluminum substrate after surface treatment. **(A)** Confocal Laser microscope image. Top view of the aluminum surface after the mechanical abrasion process. **(B)** 3D reconstructed image and topographic profile of aluminum surface after mechanical abrasion. **(C)** Picture of the surface of the AA2024T351 after abrasion process.

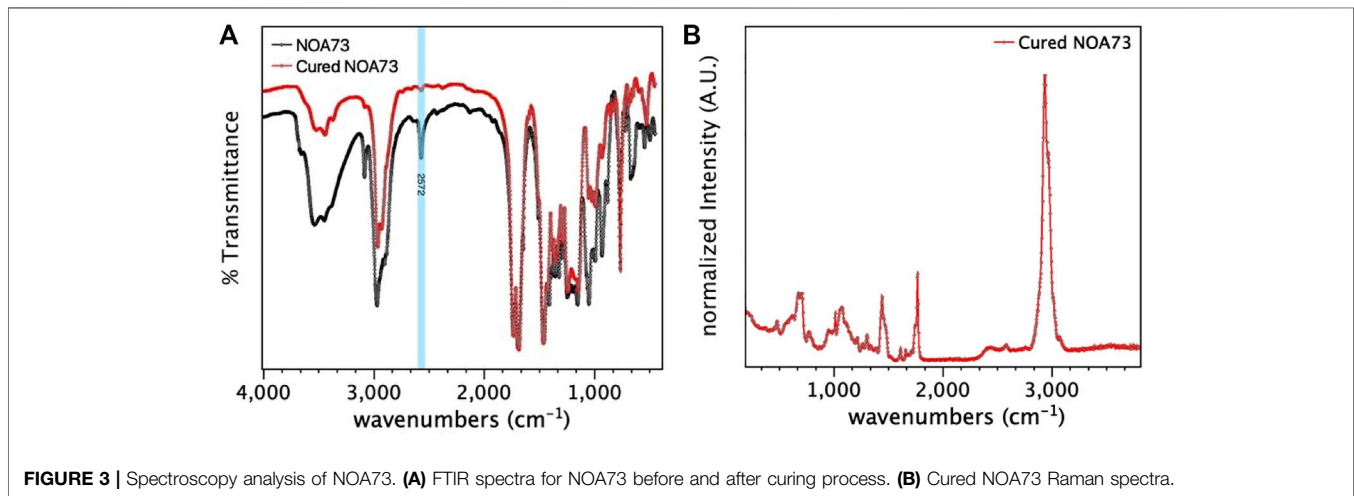


FIGURE 3 | Spectroscopy analysis of NOA73. **(A)** FTIR spectra for NOA73 before and after curing process. **(B)** Cured NOA73 Raman spectra.

TABLE 1 | Compositions of the as received Al 2024 alloy by EDAX analysis.

Element	wt%
Al	92.73
Cu	4.36
Mg	1.39
Mn	0.78
Si	0.39
Zn	0.32
Others	<0.03

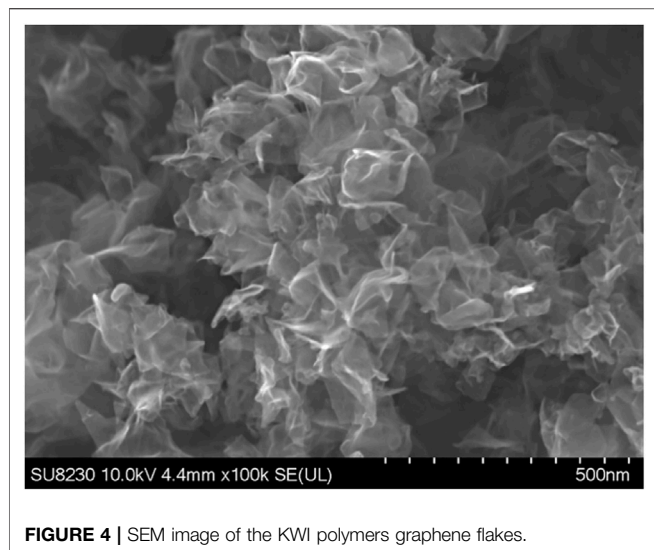
2.3 Graphene Flakes as Conductive Fillers

In this work we used porous reduced graphene flakes that were procured from KWI polymers (NDC-171107p218) and can be appreciated in **Figure 4**. Additionally, we use 100 nm Zn powder that was procured from American elements (ZN-M-02M-NP.100N). For all samples, the graphene and zinc powder were utilized as received and their incorporation into the matrix was done using magnetic stirring.

As it can be seen on **Figure 4**, the KWI graphene flakes used in this work present a voluminous corrugated structure. It is also possible to observe that the graphene flakes are semi-transparent.

2.4 Coating Preparation and Implementation

In this work we prepared two different coating formulations. The coating formulation A020 was prepared by mixing NOA73 with 2% w/w of graphene flakes and 5% w/w Zn powder. To dilute this mixture, ethanol (Sigma-Aldrich 493511) is added in the same proportion of NOA73 (1:1 mass ratio). The coating formulation A021 does not contain Zn and was prepared by mixing NOA73 with 2% w/w of graphene flakes. As before, to dilute this mixture, ethanol is added in the same proportion of NOA73 (1:1 mass ratio). It is relevant to mention that going further that 2% w/w of graphene flakes and 5% w/w Zn powder will affect the coating formulation creating a paste that is not suitable for spraying. Conversely, lower graphene concentrations did not yield the



desired anticorrosive properties that were required to pass the NSST. In **Supplementary Figure S1** in the **Supplementary Information S1**, we show the picture of a sample loaded with 1% w/w of graphene. In similar trend, less than 5% w/w zinc presence in the formulation affected the conductivity required for this specific application.

These two formulations are magnetically stirred for 5 min, then applied by spray on top of mechanically abraded aluminum samples. Deposition of the coatings is done using a SATA mini jet 4,400 spray gun with a 0.5 mm nozzle at 1.7 bar of spray pressure. We noticed that operating outside of these spraying parameters yields poor dispersion of the conductive fillers and non-uniform coatings. It is important to mention that the high load of nanofillers blocks the UV-light making the curing process longer. That is the reason why the coatings are cured at 150°C for 12 h (**Figure 5**). **Supplementary Table S1** summarizes in more detail the spray parameters and the results obtained for these coatings.

2.5 Self-Healing Mechanism

In this work we use 8-hydroxyquinoline (8HQ) as a self-healing agent that was previously reported for our team (Banerjee et al., 2020). The 8HQ was procured from Sigma Aldrich (CAS 148-24-3). A solution of 12% w/w of 8HQ in ethanol is prepared and stirred for 30 min. This solution is then sprayed atop the abraded aluminum samples and left to dry for 30 min. Finally, the top coating was sprayed and cured.

2.6 Electrical Resistance

The electrical resistance of the coatings is measured according to the standard MIL-DTL-81706B. This standard is commonly used to measure electrical resistance in chromate conversion coatings, and it is widely used in aerospace industry. The measurements were done using a standard electrical resistance system (**Figure 6**). This system uses a 4-wire connection (Kelvin method) (Kadachkar et al., 2018) (**Figures 6A, B**) to avoid measurement uncertainty that arises with two-wire connection systems.

In this method the lead (R_{lead}) resistance and contact ($R_{contact}$) resistance (**Figure 6A**) are comparable to the very low resistances of the coating (R_T). As shown in the picture (**Figure 6B**), the aluminum coated sample is placed between the two cylindrical copper electrodes of 0.5-inch diameter. A force of 200 PSI is applied using hydraulic system (**Figure 6C**) and the electrical resistance is measured cross-sectionally using a Keithley 2,400 (**Figure 6D**).

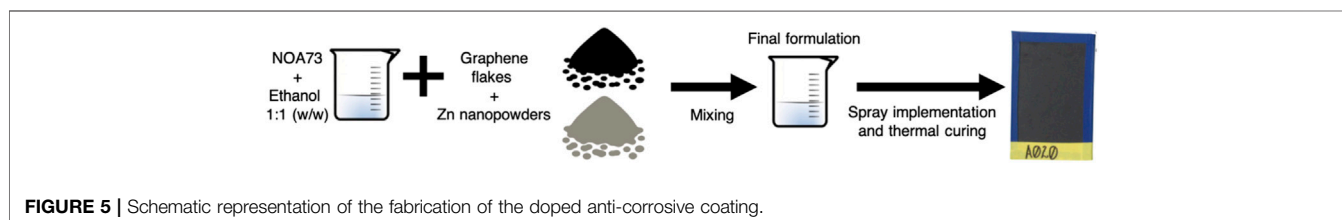
2.7 Cyclic Voltammetry

Cyclic voltammetry measurements are performed to analyze the electrochemical nature of the coating matrices. Before the measurements, pristine aluminium sample, and samples with different coating matrices (A020, A021 and A0208L) are immersed in to 5% NaCl solution for an entire day. Princeton applied research multi potentiostat instrument is used to do the cyclic voltammetry measurements with a fixed scan rate of 10 mV/s for three cycles. Silver/silver chloride, platinized grid and 5% NaCl solution are used as reference electrode, counter electrode, and electrolyte solution respectively.

3 RESULTS AND DISCUSSION

3.1 Morphological Characterization of the Coatings

To characterize the morphology of the coatings, we performed laser confocal microscope imaging, laser profilometry and SEM microscopy. The laser confocal image shows the compact and uniform surface of the A020 and A021 coatings (**Figures 7A, D** respectively). The SEM microscope image shows that A020 coating (**Figure 7B**) present a rough and crack-free surface. The SEM image for the A021 (**Figure 7E**) coating shows a smooth and crack free surface. The surface roughness for both coatings is different and can be appreciated in **Figures 7C, F**. The surface roughness parameter R_a for the A020 coating is 3.157 μm and the surface roughness parameter R_a for the A021 is 1.744 μm (**Supplementary Figures S2, 3**). This difference arises from the combination of Zn



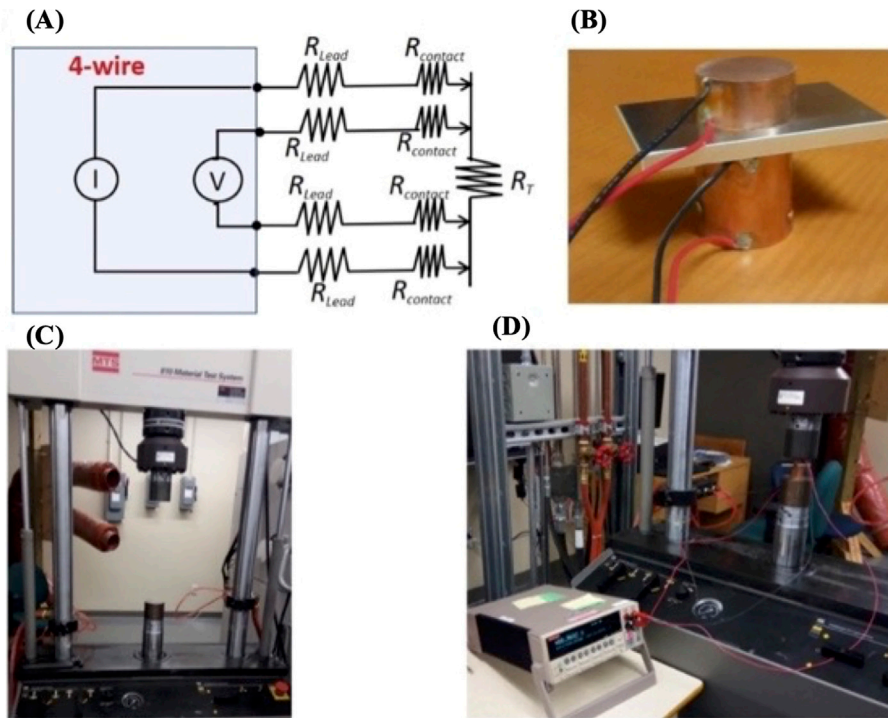


FIGURE 6 | Electrical resistance measurement system. **(A)** Schematic representation of 4-wire connection. **(B)** Image of 4-wire connection on copper electrodes. **(C)** Hydraulic system used for applying 200 pounds. **(D)** Complete measuring system following MIL-DTL-81706B.

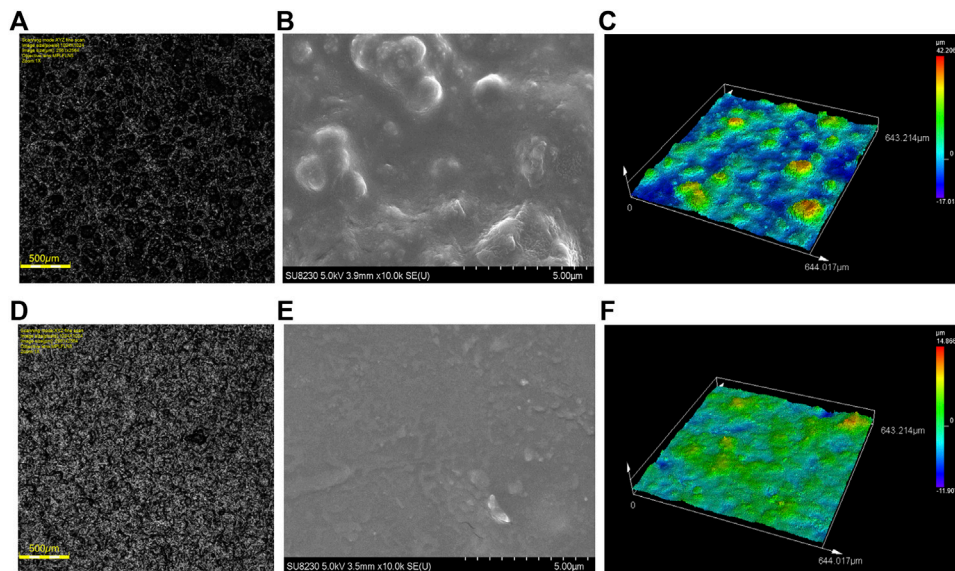


FIGURE 7 | Morphology of A020 and A021 coatings. **(A)** Confocal Laser microscope image of the A020 coating. **(B)** SEM image of the uniform and crack-free A020 coating. **(C)** Confocal Laser microscope 3D image reconstruction of the A020 coating. **(D)** Confocal Laser microscope image of the A021 coating **(E)** SEM image of the uniform and crack-free A021 coating. **(F)** Confocal Laser microscope 3D image reconstruction of the A021 coating.

nanoparticles and graphene flakes present in the A020 coating. It is important to remember that the A021 coating contains only graphene. The average thickness for both coatings is 9 μm .

These results confirm the compact nature of the coatings, which impacts positively on its anticorrosive properties (Hamdy Makhoulf, 2014). In the same way, the observed excellent

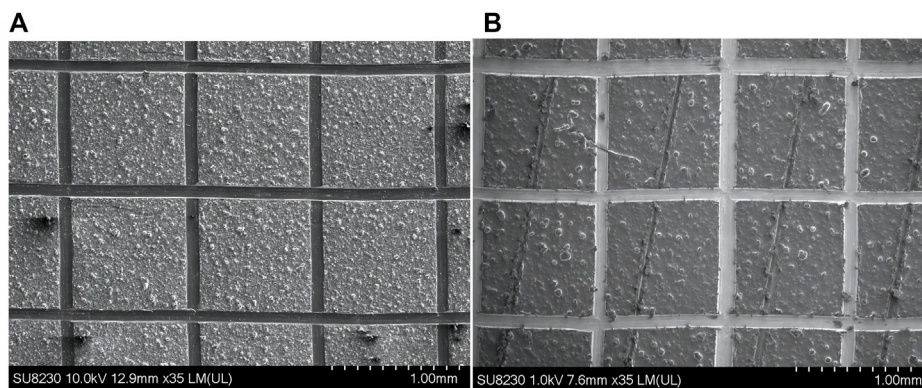


FIGURE 8 | Adhesion test. SEM image of the cross-cut test for the (A) A020 coating and (B) A021 coating.

nanofillers dispersion on both coatings is desirable since it impacts positively on the anticorrosive and low electrical resistance properties (Kim et al., 2019).

3.2 Adhesion Characterization (ISO 2409)

Adhesion test was done using a paint adhesion test (PAT) kit from Gardco (item number: PA-2000). To test the adhesion of the coating, we performed a cross-cut test following the ISO2409 standard. It is found that the A020 and A021 coatings adhesion properties are excellent. According to the standard, both coatings are class 0 since the edges of the cuts are completely smooth and all the squares of the grid are attached to the aluminum substrate. The SEM image of the samples after the crosscut test is shown in figure (Figure 8).

3.3 Electrical Resistance Characterization

The electrical resistance value obtained for the A020 coating that contains graphene and Zn ranged between 1.1 and 1.88 Ω . On the other hand, the A021 coating prepared with graphene only, displayed a resistance value around 5k Ω . The low electrical resistance values found for the A020 coating confirm that the combination of graphene and Zn enables a conductive path through all the coating. Comparing the results between samples A020 and A021, they suggest that Zn nanoparticles are responsible for bridging the graphene flakes. Thus, the electrical resistance of the A020 coating is lower. (Ramezanzadeh et al., 2017; Tian et al., 2021) (Figure 9).

As it was mentioned before, electrostatic dissipation performance arises from low electrical resistance properties. We believe that future studies for the A020 coatings should focus on testing applications in this field.

3.4 Corrosion Resistance Characterization

To evaluate the anti-corrosive properties of the A020 and A021 coatings we perform neutral salt spray test (NSSt) during 168 h at 5% saline fog. Figure 10 shows the behavior of coatings under NSSt. It is possible to observe that after 168 h both coatings maintain its integrity with no blisters or signs of corrosion.

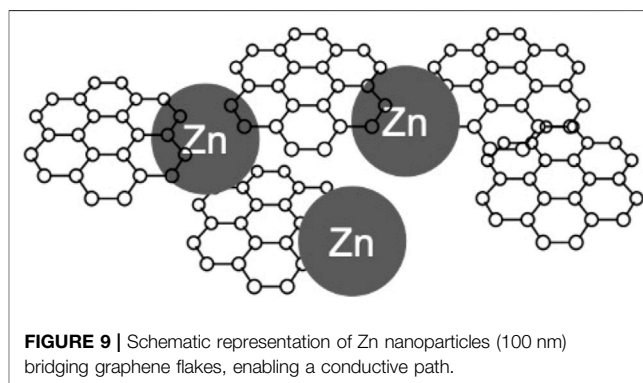


FIGURE 9 | Schematic representation of Zn nanoparticles (100 nm) bridging graphene flakes, enabling a conductive path.

Coatings containing zinc provide anticorrosive protection by two different mechanisms: one of them is behaving as anodes to provide cathodic protection to the metal substrate. This cathodic protection is possible thanks to the electron conduction path created for the graphene flakes between the Zn nanoparticles and the metallic substrate (Zhou et al., 2019). Moreover, graphene not only provides the necessary electronic channel for the anodic protection to take place, but also obstructs the diffusion path of the corrosive substances (Ding et al., 2018). In consequence the service life of the coating is extended. The second mechanism occurs when the insoluble corrosion products generated during the reaction of Zn nanoparticles seal the defects in the coating acting as an additional physical barrier against corrosive substances (Shirehjini et al., 2016).

As it was expected, for the A020 the Zn nanoparticles act as a sacrificial anodic material that retards the corrosion by oxidizing itself (Zhang, 1996) alleviating the galvanic corrosion. This Zn oxidation process yields the characteristic ZnO (Tian et al., 2021) white precipitate (Farbod and Jafarpour, 2014) that can be observed over the coating (Figure 10B). The A021 coating does not contain Zn and thus does not present the ZnO precipitate (Figure 10D).

Additional to the visual inspection, we perform Raman analysis of the coating before and after the NSSt. To this end, when the NSSt is done, the samples are rinsed with deionized

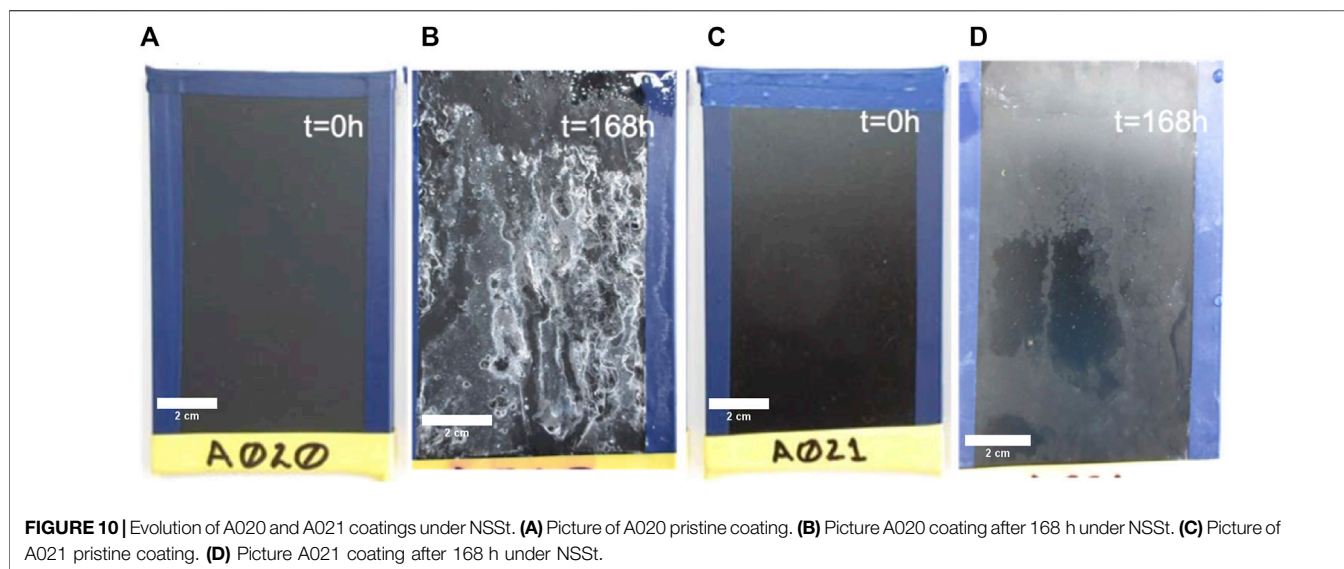


FIGURE 10 | Evolution of A020 and A021 coatings under NSSt. **(A)** Picture of A020 pristine coating. **(B)** Picture A020 coating after 168 h under NSSt. **(C)** Picture of A021 pristine coating. **(D)** Picture A021 coating after 168 h under NSSt.

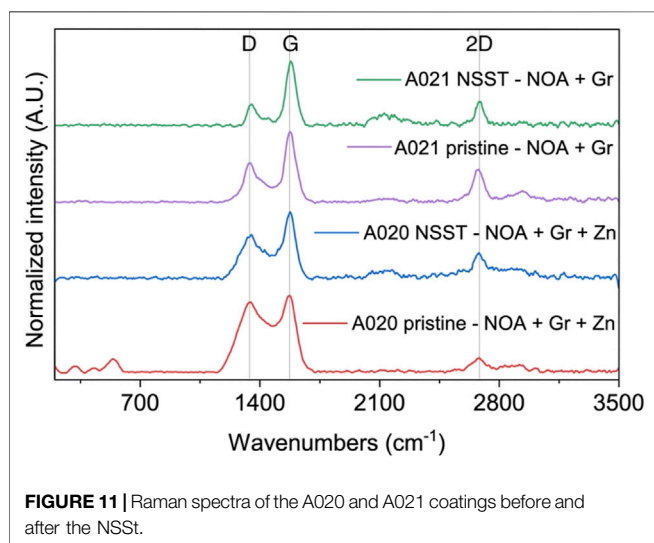


FIGURE 11 | Raman spectra of the A020 and A021 coatings before and after the NSSt.

water to expose the coating. The Raman spectra of the coatings can be appreciated in **Figure 11**.

It is interesting to observe that the graphene Raman band around $1,350\text{ cm}^{-1}$ known as the D peak (Cançado et al., 2011; Yang et al., 2017) and the band around $1,580\text{ cm}^{-1}$ known as the G peak (Cançado et al., 2011; Yang et al., 2017) show a change of their I_D/I_G ratio. The I_D/I_G ratio band represents the defects in the structure of carbon materials (Tian et al., 2021). The I_D/I_G ratio for the A020 and A021 coatings was calculated based on the intensity of these Raman bands (Cançado et al., 2011).

For the A020 coating, the pristine coating I_D/I_G ratio is 0.92 while the I_D/I_G ratio after the NSSt is 0.71. This 0.21 reduction relates to the graphene sp^2 domains that oxidize during the NSSt (Stankovich et al., 2007; Sheka et al., 2020; Tian et al., 2021). The same phenomenon was observed for the A021 coating where the pristine I_D/I_G ratio is 0.6 and the I_D/I_G ratio after the NSSt is 0.46. The 2D peak (Yang et al., 2017) around $2,684\text{ cm}^{-1}$ is typically

present in porous graphene, as is the case for the graphene used in this study for both coatings.

3.4.1 Self-Healing Capability

To further improve the anticorrosive properties, we decide to program a self-healing response on the A020 coating. To do so, we include a layer of 8HQ on top of the abraded aluminum to act as corrosion inhibitor (Andreeva et al., 2008). This self-healing mechanism is triggered when the coating experience mechanical damage such as a scratch (Banerjee et al., 2020), then this inhibitor is released and passivates the exposed aluminum by creating and insoluble chelant known as $\text{Al}(\text{HQ})_3$ that prevents corrosion (Stankiewicz et al., 2013; Zhang F. et al., 2018; Banerjee et al., 2020). This formulation is identified as A0208L.

The anti-corrosive properties for the A0208L coating were also tested under NSSt. It is important to note that the coating is scratched in the middle to evaluate the 8HQ self-healing response (**Figure 12**).

After 168 h of NSSt the characteristic white ZnO precipitate has formed over the A0208L coating (**Figure 12B**), and once again, the coating maintains its integrity with no blisters or signs of corrosion. Moreover, after rinsing the sample with deionized water to wash away the ZnO precipitate, we observe that the coating is in excellent condition and there are no signs of corrosion around the scratched area or underneath of the coating (**Figures 12C, D**). As expected, 8HQ act as corrosion inhibitor and provides self-healing capabilities under NSSt conditions (Xhanari and Finšgar, 2019; Banerjee et al., 2020).

3.4.2 Corrosion resistance by cyclic voltammetry

The lower current density values for the different coating matrices as compared to the pristine sample suggests superior anticorrosion properties from the coatings as shown in **Figure 13**.

The excellent barrier properties of the A020, A021 and A0208L coatings are expected due to the insulative nature of

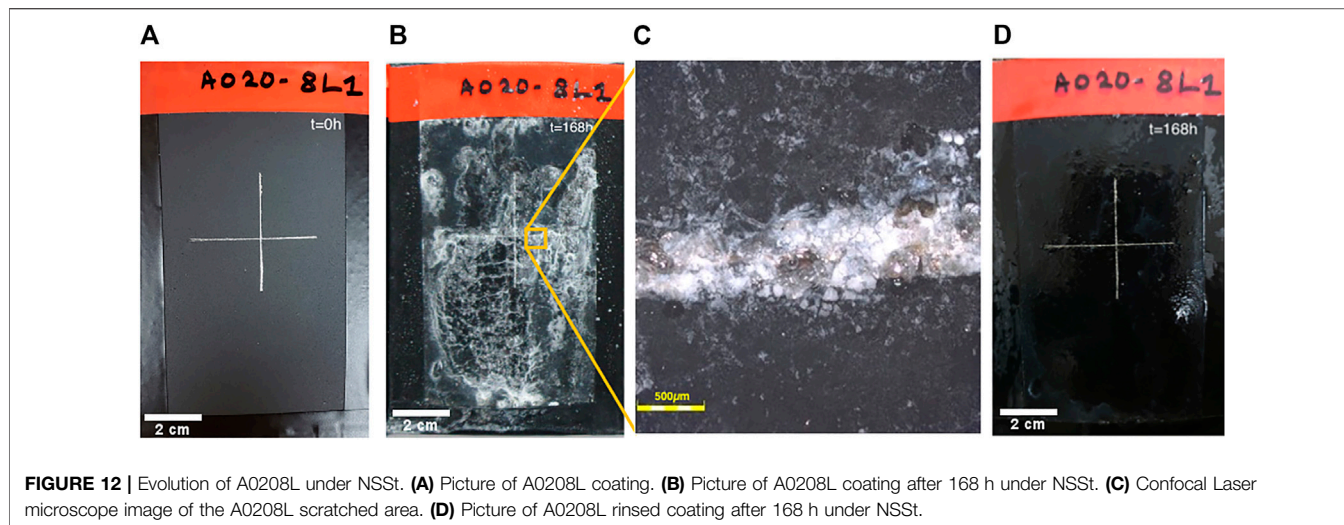


FIGURE 12 | Evolution of A0208L under NSSt. **(A)** Picture of A0208L coating. **(B)** Picture of A0208L coating after 168 h under NSSt. **(C)** Confocal Laser microscope image of the A0208L scratched area. **(D)** Picture of A0208L rinsed coating after 168 h under NSSt.

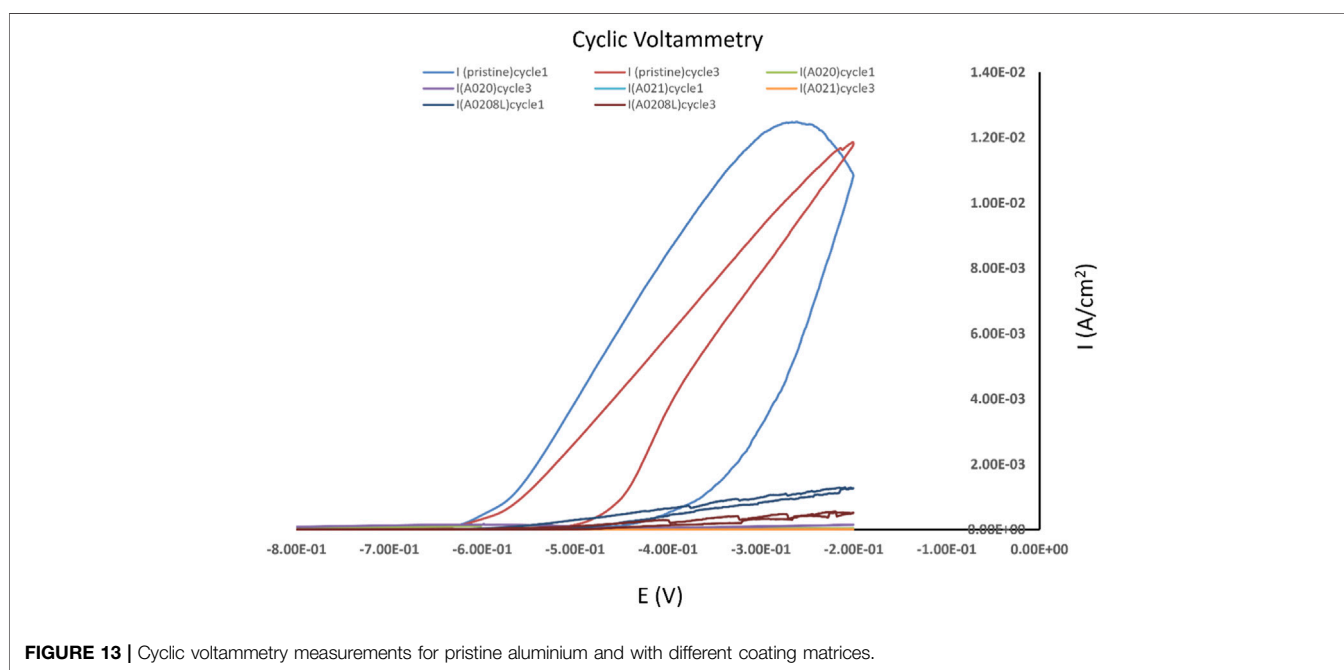


FIGURE 13 | Cyclic voltammetry measurements for pristine aluminium and with different coating matrices.

thiol-ene based polymers (Park and Braun, 2010; Wang et al., 2018, 2019) and the anticorrosion mechanism conferred by graphene (S. Aneja et al., 2015). The graphene's impermeable nature and high surface area provides an excellent barrier to water, oxygen and other corrosive compounds (S. Aneja et al., 2015). Moreover, in polymer-based coatings (A020, A021 and A0208L); graphene prevents metal/interface anodic corrosion (Böhm, 2014) by providing an alternative electrical path for the electrons, so they can't reach a cathodic site and complete the corrosion reaction (Dennis et al., 2015). As expected, dispersing graphene within an insulating (Park and Braun, 2010) resin such as NOA73 helps to prevent the galvanic coupling between the graphene flakes and the aluminum

(Alhumade et al., 2016). Furthermore, the addition of anodic materials such as zinc, helps alleviate the galvanic corrosion phenomenon (Cui et al., 2017). Finally, the 8HQ layer provides the desired self-healing response without compromising the low electrical resistance and anticorrosive properties.

The excellent integrity of the coatings after the 168 h of NSSt can be explained based on the behavior of graphene-resin composite coatings that display improved mechanical properties, more durability and scratch-resistance (Dennis et al., 2013). Coatings with well-dispersed graphene flakes ensure low electrical resistivity and low overall permeability to gas or liquid (Böhm, 2014).

4 CONCLUSION

In summary, a coating technology with low electrical resistance, anticorrosive properties and self-healing capabilities was demonstrated. First, a FTIR and Raman analysis were used to obtain information about the nature of NOA73 and its selection as a host matrix for the conductive fillers (graphene flakes and Zn nanopowders). The clever combination of the anticorrosive properties of graphene with NOA73 provides excellent anticorrosive response as expected. The addition of Zn nanoparticles helps to enable a low electrical resistance path while performing as well as a sacrificial material. The coatings presented in this work are applied using spray gun and tested under the current industrial standards. It is found that formulation A020 containing graphene and Zn nanoparticles as conductive fillers, performs as an excellent anti-corrosion and low electrical resistance coating. Its anti-corrosive properties are tested during 168 h under natural salt spray test. They presented ZnO deposition and no signs of corrosion. The A020 coating's low electrical resistance is explained thanks to the inclusion on Zn nanoparticles that bridge the graphene flakes enabling a conductive path. Similarly, formulation A021 containing graphene only, provide excellent anticorrosive properties but high electrical resistance. The programmed self-healing response was successfully tested during NSSt. It showed no signs of corrosion after 168 h and help to boots the service life of the coatings. Cyclic voltammetry was used to confirm the excellent barrier properties of the A020, A021 and A0208L coatings confirming the excellent blocking properties of the tested coatings.

We believe this smart coating technology is compatible with aerospace applications but can have a significant impact in other areas such as automotive, construction, submarines etc. However, spray coating implementation at specific parameters is crucial to

achieve an excellent anticorrosive and mechanical properties along with low electrical resistance.

DATA AVAILABILITY STATEMENT

The original contributions presented in the study are included in the article/**Supplementary Material**, further inquiries can be directed to the corresponding author.

AUTHOR CONTRIBUTIONS

JB-G, DB, DG and SC developed the concept of the coating. JB-G, DB and DG, performed the samples preparation and experiments. JB-G, DB, DG and LG performed the samples characterization such as Raman, SEM, LEXT, NSST and cyclic voltammetry. Interpretations of the results and data analysis were discussed between all the authors. The first draft of the manuscript was written by JB-G and revised by DB, LG and SC All authors have approved the final version of the manuscript before its submission.

ACKNOWLEDGMENTS

SC is most thankful to ArianeGroup, PRIMA-Quebec and the Canada Research Chair program for their financial support.

SUPPLEMENTARY MATERIAL

The Supplementary Material for this article can be found online at: <https://www.frontiersin.org/articles/10.3389/fmats.2022.835855/full#supplementary-material>

REFERENCES

- Aal, N. A., El-Tantawy, F., Al-Hajry, A., and Bououdina, M. (2008). New Antistatic Charge and Electromagnetic Shielding Effectiveness from Conductive Epoxy Resin/plasticized Carbon Black Composites. *Polym. Compos.* 29, 125–132. doi:10.1002/pc.20334
- Agustín-Sáenz, C., Santa Coloma, P., Fernández-Carretero, F. J., Brusciotti, F., and Brizuela, M. (2020). Design of Corrosion Protective and Antistatic Hybrid Sol-Gel Coatings on 6XXX AlMgSi Alloys for Aerospace Application. *Coatings* 10, 441. doi:10.3390/coatings10050441
- Alhumade, H., Abdala, A., Yu, A., Elkamel, A., and Simon, L. (2016). Corrosion Inhibition of Copper in Sodium Chloride Solution Using Polyetherimide/graphene Composites. *Can. J. Chem. Eng.* 94, 896–904. doi:10.1002/cjce.22439
- Andreeva, D. V., Fix, D., M'ohwald, H., and Shchukin, D. G. (2008). Self-Healing Anticorrosion Coatings Based on pH-Sensitive Polyelectrolyte/Inhibitor Sandwichlike Nanostructures. *Adv. Mater.* 20, 2789–2794. doi:10.1002/adma.200800705
- Aneja, K. S. K., Bohm, S., Khanna, A. S., and Bohm, H. L. M. (2015). Graphene Based Anticorrosive Coatings for Cr(vi) Replacement. *Nanoscale* 7, 17879–17888. doi:10.1039/C5NR04702A
- Banerjee, D., Guo, X., Benavides, J., Rameau, B., and Cloutier, S. G. (2020). Designing green Self-Healing Anticorrosion Conductive Smart Coating for Metal protection. *Smart Mater. Struct.* 29, 105027. doi:10.1088/1361-665X/aba849
- Barsoum, M., and Barsoum, M. W. (2002). *Fundamentals of Ceramics*. Boca Raton: CRC Press.
- Böhm, S. (2014). Graphene against Corrosion. *Nat. Nanotech* 9, 741–742. doi:10.1038/nnano.2014.220
- Cançado, L. G., Jorio, A., Ferreira, E. H. M., Stavale, F., Achete, C. A., Capaz, R. B., et al. (2011). Quantifying Defects in Graphene via Raman Spectroscopy at Different Excitation Energies. *Nano Lett.* 11, 3190–3196. doi:10.1021/nl201432g
- Chou, T. P., Chandrasekaran, C., and Cao, G. Z. (2003). Sol-Gel-Derived Hybrid Coatings for Corrosion Protection. *J. Sol-gel Sci. Technol.* 26, 321–327. doi:10.1023/A:1020736107842
- Cui, C., Lim, A. T. O., and Huang, J. (2017). A Cautionary Note on Graphene Anticorrosion Coatings. *Nat. Nanotech* 12, 834–835. doi:10.1038/nnano.2017.187
- Davis, J. R. (1999). *Corrosion of Aluminum and Aluminum Alloys*. USA: ASM International.
- Dennis, R., Viyannalage, L., Gaikwad, A., Rout, T., and Banerjee, S. (2013). Graphene Nanocomposite Coatings for Protecting Lowalloy Steels from Corrosion. *Am. Ceram. Soc. Bull.* 92 (5), 18–24.
- Dennis, R. V., Patil, V., Andrews, J. L., Aldinger, J. P., Yadav, G. D., and Banerjee, S. (2015). Hybrid Nanostructured Coatings for Corrosion protection of Base Metals: a Sustainability Perspective. *Mater. Res. Express* 2, 032001. doi:10.1088/2053-1591/2/3/032001
- Ding, R., Zheng, Y., Yu, H., Li, W., Wang, X., and Gui, T. (2018). Study of Water Permeation Dynamics and Anti-corrosion Mechanism of Graphene/zinc Coatings. *J. Alloys Comp.* 748, 481–495. doi:10.1016/j.jallcom.2018.03.160

- Farbod, M., and Jafarpoor, E. (2014). Hydrothermal Synthesis of Different Colors and Morphologies of ZnO Nanostructures and Comparison of Their Photocatalytic Properties. *Ceramics Int.* 40, 6605–6610. doi:10.1016/j.ceramint.2013.11.116
- Gvishi, R., Strum, G., and Englander, A. (2012). UV-curable Glassy Material for the Manufacture of Bulk and Nano-Structured Elements. *JEOS:RP* 7, 2002, doi:10.2971/jeos.2012.12002
- Hamdy, A. S. (2007). Alkaline-Based Surface Modification Prior to Ceramic-Based Cerate Conversion Coatings for Magnesium AZ91D. *Electrochem. Solid-state Lett.* 10, C21. doi:10.1149/1.2430565
- Hamdy, A. S. (2006). Advanced Nano-Particles Anti-corrosion Ceria Based Sol Gel Coatings for Aluminum Alloys. *Mater. Lett.* 60, 2633–2637. doi:10.1016/j.matlet.2006.01.049
- Hamdy, A. S., and Beccaria, A. M. (2005). Effect of Surface Preparation Prior to Cerium Pre-treatment on the Corrosion protection Performance of Aluminum Composites. *J. Appl. Electrochem.* 35, 473–478. doi:10.1007/s10800-004-8330-x
- Hamdy, A. S., Doench, I., and Möhwal, H. (2011). Assessment of a One-step Intelligent Self-Healing Vanadia Protective Coatings for Magnesium Alloys in Corrosive media. *Electrochimica Acta* 56, 2493–2502. doi:10.1016/j.electacta.2010.11.103
- Hamdy, A. S., Doench, I., and Möhwal, H. (2012). The Effect of Alkaline Etching Time on the Anticorrosion Performance of Vanadia Film Formed on High Strength AA2024 in Chloride media. *J. Mater. Sci.* 47, 3784–3792. doi:10.1007/s10853-011-6232-y
- Hamdy, A. S., and Farahat, M. (2010). Chrome-free Zirconia-Based Protective Coatings for Magnesium Alloys. *Surf. Coat. Tech.* 204, 2834–2840. doi:10.1016/j.surfcoat.2010.02.063
- Hamdy, A. S. (2008). The Effect of Surface Modification and Stannate Concentration on the Corrosion protection Performance of Magnesium Alloys. *Surf. Coat. Tech.* 203, 240–249. doi:10.1016/j.surfcoat.2008.08.070
- Hamdy Makhlof, A. S. (2014). *Handbook of Smart Coatings for Materials Protection* Cambridge: Woodhead Publishing.
- Han, Y.-H., Taylor, A., Mantle, M. D., and Knowles, K. M. (2007). Sol-gel-derived Organic-Inorganic Hybrid Materials. *J. Non-Crystalline Sol.* 353, 313–320. doi:10.1016/j.jnoncrysol.2006.05.042
- Heusler, K. E., Landolt, D., and Trasatti, S. (1989). Electrochemical Corrosion Nomenclature (Recommendations 1988). *Pure Appl. Chem.* 61, 19–22. doi:10.1351/pac198961010019
- Hou, B., Li, X., Ma, X., Du, C., Zhang, D., Zheng, M., et al. (2017). The Cost of Corrosion in China. *Npj Mater. Degrad.* 1, 1–10. doi:10.1038/s41529-017-0005-2
- Ireni, N. G., Narayan, R., Basak, P., and Raju, K. V. S. N. (2016). Poly(thiourethane-urea) as Anticorrosion Coatings with Impressive Optical Properties. *Polymer* 97, 370–379. doi:10.1016/j.polymer.2016.04.072
- Jang, J. (2006). “Conducting Polymer Nanomaterials and Their Applications,” in *Emissive Materials Nanomaterials Advances in Polymer Science* (Berlin, Heidelberg: Springer), 189–260. doi:10.1007/12_075
- Kadechkar, A., Riba, J.-R., Moreno-Eguilaz, M., Capelli, F., and Gonzalez, D. (2018). “On-line Resistance Measurement of Substation Connectors Focused on Predictive Maintenance,” in *IEEE 18th International Power Electronics and Motion Control Conference, Budapest, Hungary, 26-30 Aug. 2018* (Budapest: IEEE), 846–851. doi:10.1109/EPEPEMC.2018.8521913
- Katzman, H. A., Malouf, G. M., Bauer, R., and Stupian, G. W. (1979). Corrosion-protective Chromate Coatings on Aluminum. *Appl. Surf. Sci.* 2, 416–432. doi:10.1016/0378-5963(79)90073-4
- Kendig, M. W., and Buchheit, R. G. (2003). Corrosion Inhibition of Aluminum and Aluminum Alloys by Soluble Chromates, Chromate Coatings, and Chromate-free Coatings. *CORROSION* 59, 379–400. doi:10.5006/1.3277570
- Kim, H., Lee, H., Lim, H.-R., Cho, H.-B., and Choa, Y.-H. (2019). Electrically Conductive and Anti-corrosive Coating on Copper Foil Assisted by Polymer-Nanocomposites Embedded with Graphene. *Appl. Surf. Sci.* 476, 123–127. doi:10.1016/j.apsusc.2019.01.066
- Larsson, A. (2002). The Interaction between a Lightning Flash and an Aircraft in Flight. *Comptes Rendus Physique* 3, 1423–1444. doi:10.1016/S1631-0705(02)01410-X
- Mackenzie, J. D., and Bescher, E. P. (1998). Structures, Properties and Potential Applications of Ormosils. *J. Sol-gel Sci. Technol.* 13, 371–377. doi:10.1023/A:1008600723220
- Makhlof, A. S. H., and Tiginyanu, I. (2011). *Nanocoatings and Ultra-thin Films: Technologies and Applications*. Cambridge: Woodhead Publishing.
- Metroke, T. L., Kachurina, O., and Knobbe, E. T. (2002). Spectroscopic and Corrosion Resistance Characterization of GLYMO-TEOS Ormosil Coatings for Aluminum alloy Corrosion Inhibition. *Prog. Org. Coat.* 44, 295–305. doi:10.1016/S0300-9440(02)00063-2
- Mondolfo, L. F. (2013). *Aluminum Alloys: Structure and Properties*. London: Elsevier.
- Mongkhontreerat, S., Öberg, K., Erixon, L., Löwenhielm, P., Hult, A., and Malkoch, M. (2013). UV Initiated Thiol-Ene Chemistry: a Facile and Modular Synthetic Methodology for the Construction of Functional 3D Networks with Tunable Properties. *J. Mater. Chem. A* 1, 13732–13737. doi:10.1039/C3TA12963B
- Nagarjuna, R., Saifullah, M. S. M., and Ganesan, R. (2018). Oxygen Insensitive Thiol-Ene Photo-Click Chemistry for Direct Imprint Lithography of Oxides. *RSC Adv.* 8, 11403–11411. doi:10.1039/C8RA01688G
- Nazeer, A. A., and Madkour, M. (2018). Potential Use of Smart Coatings for Corrosion protection of Metals and Alloys: A Review. *J. Mol. Liquids* 253, 11–22. doi:10.1016/j.molliq.2018.01.027
- O'Brien, P., and Kortenkamp, A. (1995). The Chemistry Underlying Chromate Toxicity. *Transit. Met Chem* 20, 636–642. doi:10.1007/BF00136433
- Pagliaro, M., Ciriminna, R., and Palmisano, G. (2009). Silica-based Hybrid Coatings. *J. Mater. Chem.* 19, 3116–3126. doi:10.1039/B819615J
- Pan, C., Wang, X., Behnamian, Y., Wu, Z., Qin, Z., Xia, D.-H., et al. (2020). Monododecyl Phosphate Film on LY12 Aluminum Alloy: pH-Controlled Self-Assembly and Corrosion Resistance. *J. Electrochem. Soc.* 167, 161510. doi:10.1149/1945-7111/abd3bb
- Park, J.-H., and Braun, P. V. (2010). Coaxial Electrospinning of Self-Healing Coatings. *Adv. Mater.* 22, 496–499. doi:10.1002/adma.200902465
- Ramezanzadeh, B., Mohamadzadeh Moghadam, M. H., Shohani, N., and Mahdavian, M. (2017). Effects of Highly Crystalline and Conductive Polyaniline/graphene Oxide Composites on the Corrosion protection Performance of a Zinc-Rich Epoxy Coating. *Chem. Eng. J.* 320, 363–375. doi:10.1016/j.cej.2017.03.061
- Resetco, C., Hendriks, B., Badi, N., and Du Prez, F. (2017). Thiol-ene Chemistry for Polymer Coatings and Surface Modification - Building in Sustainability and Performance. *Mater. Horiz.* 4, 1041–1053. doi:10.1039/C7MH00488E
- Sanoria, A., Ulbricht, D., Schuster, T., and Brüll, R. (2015). Monitoring Crosslinking Inhomogeneities in Ethylene Vinyl Acetate Photovoltaic Encapsulants Using Raman Microscopy. *RSC Adv.* 5, 93522–93529. doi:10.1039/C5RA18988H
- Sheka, E. F., Golubev, Y. A., and Popova, N. A. (2020). Graphene Domain Signature of Raman Spectra of Sp² Amorphous Carbons. *Nanomaterials* 10, 2021. doi:10.3390/nano10102021
- Shi, X., Nguyen, T. A., Suo, Z., Liu, Y., and Avci, R. (2009). Effect of Nanoparticles on the Anticorrosion and Mechanical Properties of Epoxy Coating. *Surf. Coat. Tech.* 204, 237–245. doi:10.1016/j.surfcoat.2009.06.048
- Shirehjini, F. T., Danaee, I., Eskandari, H., and Zarei, D. (2016). Effect of Nano Clay on Corrosion Protection of Zinc-Rich Epoxy Coatings on Steel 37. *J. Mater. Sci. Tech.* 32, 1152–1160. doi:10.1016/j.jmst.2016.08.017
- Smitha, V. S., Syamili, S. S., Nair, B. N., Hareesh, U. S., and Hareesh, S. U. (2018). ORMOSIL-ZrO₂ Hybrid Nanocomposites and Coatings on Aluminium Alloys for Corrosion Resistance; a Sol-Gel Approach. *New J. Chem.* 42, 10337–10347. doi:10.1039/C7NJ05174C
- Sorensen, P. A., Kiil, S., Dam-Johansen, K., and Weinell, C. E. (2009). Anticorrosive Coatings: a Review. *J. Coat. Technol. Res.* 6, 135–176. doi:10.1007/s11998-008-9144-2
- Stankiewicz, A., Szczygiel, I., and Szczygiel, B. (2013). Self-healing Coatings in Anti-corrosion Applications. *J. Mater. Sci.* 48, 8041–8051. doi:10.1007/s10853-013-7616-y
- Stankovich, S., Dikin, D. A., Piner, R. D., Kohlhaas, K. A., Kleinhammes, A., Jia, Y., et al. (2007). Synthesis of Graphene-Based Nanosheets via Chemical Reduction of Exfoliated Graphite Oxide. *Carbon* 45, 1558–1565. doi:10.1016/j.carbon.2007.02.034
- Tian, Y., Bi, Z., and Cui, G. (2021). Study on the Corrosion Resistance of Graphene Oxide-Based Epoxy Zinc-Rich Coatings. *Polymers* 13, 1657. doi:10.3390/polym13101657
- Tiwari, A., Hihara, L., and Rawlins, J. (2014). *Intelligent Coatings for Corrosion Control*. Boston: Butterworth-Heinemann.
- Wang, H., He, Y., Fei, G., Wang, C., Shen, Y., Zhu, K., et al. (2019). Functionalizing Graphene with Titanate Coupling Agents as Reinforcement for One-

- Component Waterborne Poly(urethane-Acrylate) Anticorrosion Coatings. *Chem. Eng. J.* 359, 331–343. doi:10.1016/j.cej.2018.11.133
- Wang, H., Qin, S., Yang, X., Fei, G., Tian, M., Shao, Y., et al. (2018). A Waterborne Uniform Graphene-Poly(urethane-Acrylate) Complex with Enhanced Anticorrosive Properties Enabled by Ionic Interaction. *Chem. Eng. J.* 351, 939–951. doi:10.1016/j.cej.2018.06.151
- Xhanari, K., and Finšgar, M. (2019). Organic Corrosion Inhibitors for Aluminum and its Alloys in Chloride and Alkaline Solutions: A Review. *Arabian J. Chem.* 12, 4646–4663. doi:10.1016/j.arabj.2016.08.009
- Xia, D.-H., Pan, C., Qin, Z., Fan, B., Song, S., Jin, W., et al. (2020). Covalent Surface Modification of LY12 Aluminum alloy Surface by Self-Assembly Dodecyl Phosphate Film towards Corrosion protection. *Prog. Org. Coat.* 143, 105638. doi:10.1016/j.porgcoat.2020.105638
- Yadav, R., Tirumali, M., Wang, X., Naebe, M., and Kandasubramanian, B. (2020). Polymer Composite for Antistatic Application in Aerospace. *Defence Tech.* 16, 107–118. doi:10.1016/j.dt.2019.04.008
- Yang, S., Yang, Y., He, P., Wang, G., Ding, G., and Xie, X. (2017). Insights into the Oxidation Mechanism of Sp²-Sp³ Hybrid Carbon Materials: Preparation of a Water-Soluble 2D Porous Conductive Network and Detectable Molecule Separation. *Langmuir* 33, 913–919. doi:10.1021/acs.langmuir.6b03937
- Zang, D., Zhu, R., Zhang, W., Wu, J., Yu, X., and Zhang, Y. (2014). Stearic Acid Modified Aluminum Surfaces with Controlled Wetting Properties and Corrosion Resistance. *Corrosion Sci.* 83, 86–93. doi:10.1016/j.corsci.2014.02.003
- Zhang, F., Ju, P., Pan, M., Zhang, D., Huang, Y., Li, G., et al. (2018a). Self-healing Mechanisms in Smart Protective Coatings: A Review. *Corrosion Sci.* 144, 74–88. doi:10.1016/j.corsci.2018.08.005
- Zhang, Q., Liu, L., Pan, C., and Li, D. (2018b). Review of Recent Achievements in Self-Healing Conductive Materials and Their Applications. *J. Mater. Sci.* 53, 27–46. doi:10.1007/s10853-017-1388-8
- Zhang, X. G. (1996). Galvanic Corrosion of Zinc and its Alloys. *J. Electrochem. Soc.* 143, 1472–1484. doi:10.1149/1.1836662
- Zhou, S., Wu, Y., Zhao, W., Yu, J., Jiang, F., Wu, Y., et al. (2019). Designing Reduced Graphene Oxide/zinc Rich Epoxy Composite Coatings for Improving the Anticorrosion Performance of Carbon Steel Substrate. *Mater. Des.* 169, 107694. doi:10.1016/j.matdes.2019.107694

Conflict of Interest: The authors declare that the research was conducted in the absence of any commercial or financial relationships that could be construed as a potential conflict of interest.

Publisher's Note: All claims expressed in this article are solely those of the authors and do not necessarily represent those of their affiliated organizations, or those of the publisher, the editors and the reviewers. Any product that may be evaluated in this article, or claim that may be made by its manufacturer, is not guaranteed or endorsed by the publisher.

Copyright © 2022 Benavides-Guerrero, Banerjee, Gedamu, Gerlein and Cloutier. This is an open-access article distributed under the terms of the Creative Commons Attribution License (CC BY). The use, distribution or reproduction in other forums is permitted, provided the original author(s) and the copyright owner(s) are credited and that the original publication in this journal is cited, in accordance with accepted academic practice. No use, distribution or reproduction is permitted which does not comply with these terms.